Mining of Mineral Deposits
Volume 18 (2024), Issue 2, 71-82

MMD JOURNAL / MINING.IN.UA

https://doi.org/10.33271/mining18.02.071

Research into mechanical properties of ore and rocks in the ore deposits with assessment of the mass stress state natural field

Azamat Matayev [1], Sholpan Zeitinova [1*], Ravil Mussin [1], Dinara Doni [1], Nurlan Shaike [1], Aidar Kuttybayev [2*], Rustem Iskakov [1]

[1] *Abylkas Saginov Karaganda Technical University, Karaganda, Kazakhstan*
[2] *Satbayev University, Almaty, Kazakhstan*

**Corresponding author: e-mail sh.zeytinova@kstu.kz, a.kuttybayev@satbayev.university*

Abstract

Purpose. The research aims to conduct a comprehensive study of the mechanical properties of ores and rocks within the Zhilandy Group field, as well as to assess the natural field of mass stress state to solve geomechanical problems in optimizing mining operations.

Methods. To determine the boundary conditions when measuring the stress-strain state of the mass, a complex methodology is proposed, including stress measurements using hydraulic fracturing methods of the wells and determining the physical-mechanical properties of rocks. Five rock probes have been tested. Twelve tests (six tests in natural and six in water-saturated states) have been conducted for each probe.

Findings. Hydraulic fracturing tests at the metering stations show significant tectonic stress due to the shape of structural folds and the mass fracturing. It has been revealed that the hard rock mass is characterized by non-uniform fracturing. It is of tectonic origin and averages between 10-15 and 15-25 fractures per meter for different lithological varieties. The maximum horizontal stress at the stations is oriented along an azimuth of 70° ± 10.

Originality. The influence of water saturation on the reduction of strength and deformation characteristics of rocks has been determined for the conditions of the Zhilandy Group field, which shows significant variations depending on the rock type. Especially important is the revealed fact of a significant decrease in uniaxial compression and uniaxial tensile strength, as well as a decrease in Young's modulus and cohesion factor. Linear dependences of stresses occurring with depth have been obtained from the measurement results.

Practical implications. The results obtained are of significant importance for the mining industry. Understanding the extent of reduction in strength characteristics during water saturation and assessing the natural field of the stress mass state allows more accurate prediction of rock behavior.

Keywords: *stress state of the mass, ore, rock, numerical analysis, fracturing*

1. Introduction

In the depths of Kazakhstan, about 100 types of minerals have been found, which is due to the favorable geographical position of the country, including a variety of geological structures and different types of rocks formed over a long period of time – from ancient Archean formations to young Quaternary deposits [1]-[3].

The geological diversity of Kazakhstan is important for the location of the main types of minerals in its different regions [4]-[8]:

1. North Kazakhstan Region is the main one for aluminium, gold and iron ore mining. There are also large reserves of nickel-cobalt, tin-tantalum and titanium-zirconium ores, as well as a chrysotile-asbestos deposit. Industrial grade diamond deposit is also expected to be mined, and the Shaymerden field contains unique zinc reserves.

2. East Kazakhstan Region is known for its polymetallic deposits, including gold, lead, zinc, copper and rare elements. This region also contains significant titanium ore reserves.

3. Central Kazakhstan Region is a major supplier of copper and manganese. Coal basins, tungsten-molybdenum and lead-zinc ores are also located here.

4. South Kazakhstan Region has unique uranium deposits, which are mined using high-tech in-situ leaching methods, and is also an important region for phosphate raw materials.

5. West Kazakhstan Region is rich in oil, gas, potassium salts, boron and chromite.

Thus, the diversity of geological formations in Kazakhstan determines its wealth of various mineral resources in different regions of the country [9]. Mining industry of the Republic of Kazakhstan has become one of the most competitive industries in the country, having achieved stable growth at the beginning of the XXI century. This success is largely

Received: 15 February 2024. Accepted: 3 June 2024. Available online: 30 June 2024

Mining of Mineral Deposits. ISSN 2415-3443 (Online) | ISSN 2415-3435 (Print)

due to attracting foreign investment to develop this sector of the economy [10]-[13].

With the development of the mining industry and the ever-increasing depth of mining, new challenges are emerging. These challenges highlight the importance of improving mining equipment and tools based on achievements in materials science [14]-[19].

The rock mass stress-strain state influenced by mining operations can change significantly, which will have a negative impact on the stability of underground mine workings [20], [21]. Redistribution of stresses acting in the mass may adversely affect the stability of underground mine workings, which entails capital expenditures for their fastening. The complexity of mining-geological conditions also has a significant impact on the stability of mine workings and imposes quite strict requirements for the design of preparatory and stope operations [22]. Under such conditions, the importance of the problem of preventing negative rock pressure manifestations and ensuring the stability of mine workings is becoming increasingly important, the solution of which requires information about the natural stress field [23]-[25]. Therefore, the assessment of the stress state of rocks in the mass is an urgent task.

In order to solve geomechanical problems such as rock mass state management, maintenance of mine workings in a stable state and their safe operation, a broader study of rock behavior in the border mass part is required. This will provide reliable and timely information on the stress-strain state dynamics of the mass adjacent to mine workings [26], [27].

The Zhilandy Group field is confined to the western, north-western, north-eastern and eastern wings of the Zhezkazgan syncline. The manifestation of Hercynian tectogenesis has led to the formation here of structures of the 2nd and higher orders (domes, troughs), complicated by longitudinal flexural compression zones and disjunctive faults. The Zhilandy Group field is located 30-35 km north of the Zhezkazgan mines and comprises 5 fields (west to east): Itauz, West Saryoba, East Saryoba, Kipshakpai, and North Karashoshak (Fig. 1). In general, the fields are characterized by a complex geological structure, which is especially true for large ones: East Saryoba, West Saryoba and Itauz. These areas are the zones of the highest stresses, which have led to the formation of both folding and discontinuity faults.

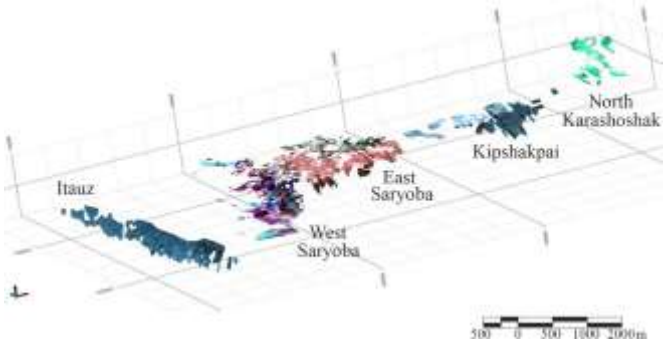

Figure 1. Zhilandy Group field

A characteristic peculiarity of the localization of mineralization within the Zhilandy Group field is the multi-tiered occurrence of predominantly conformable seam-shaped ore deposits. Industrial mineralization is typically confined to seams of grey-colored sandstones, conglomerates and, less commonly, grey, dark grey and black siltstones. Ore deposits are characterized by highly variable thickness and non-uniform distribution of useful components. In plan, the ore bodies have a cloak-like, rounded-elongated, ribbon-like shape, often characterized by rather complex contours. On the flanks or in the inner part they are broken up by waste rocks or off-balance ores [28], [29].

Mineralization has a typical disseminated and vein-like disseminated character. The main ore-forming minerals in the primary ore zone are chalcosine, bornite, chalcopyrite, galena and sphalerite. Among the minerals of oxidized ores, malachite, azurite, and native copper are found. The lower ore-bearing horizons, along with copper minerals, are characterized by dense dissemination and accumulations of pyrite, fahlite, galena, and arsenopyrite. The secondary sulphide beneficiation zone extends to a depth of 40-100 m from the daylight surface and contains predominantly chalcosine ores. Bornite, covelline, and rarely native copper are observed in subordinate amounts here. The oxidation zone in the East Saryoba field is manifested only in the zone of the Central Saryoba transpressional fault, where ore bodies as a result of overthrust displacements are moved to the near-surface part. Structurally, the Saryoba ore field, within which the deposit is located, is confined to the shallow dipping area of the Zhezkazgan syncline northern flank, which is complicated by higher-order folds and differently orientated discontinuity faults.

The Itauz field is represented by subvertical ore bodies with a thickness of a few meters to 25 m. Typically, ore bodies are 5-10 m thick. The geological structure includes fine-grained siltstones and argillites, as well as coarse-grained sandstones with rare interlayers of intraformational conglomerates. The occurrence of rocks is steeply dipping of 75-80°. The rocks are fractured by a series of secant interstratial and intrastratal fractures. The fractures are filled with calcite, cavities or crushed material. The upper part of the field is quarried. Underground mining is currently being conducted by a sub-level caving system.

The West Saryoba field is confined to flat-lying part of the Zhezkazgan syncline northern flank. The mass structure is similar to chest folds with almost horizontal occurrence in the cores and steeply dipping wings; it is complicated by longitudinal steeply dipping tectonic zones such as flexures of a higher order, in some places with rock discontinuity.

The East Saryoba field is represented by flat-dipping (10-20°) of medium and low thickness deposits with a dip to the south. In the southern part, the dip angle of deep horizons increases to 50-60°. The East Saryoba field is penetrated by inclined slopes from the surface.

The East Saryoba and West Saryoba fields are divided into approximately two equal parts by the Central Saryoba discontinuity fault zone. It extends in meridional direction for 4 km and is 400-600 m wide in the north and 1000-1200 m wide in the south. The zone has a block structure and dips to the west at angles of 25-40°. At the same time, the western block is thrust over the eastern block. The vertical displacement amplitude is 280-300 m, and the horizontal displacement is 3 km.

The Kipshakpai field is a continuation of the East Saryoba field with intermittent mineralization. The northern flanks dip south at angles of 10-20°. To the south, they dip at steeper angles of 40-50°.

The North Karashoshak field is located on the north-eastern flank of the Karashoshak syncline. The rock seams

dip to the southeast at an angle of 13-47°. On the daylight surface, the rocks outcrop in linear ridges, elongated in the north-eastern direction (azimuth of 50-600 m). Mineralization occurs in two ore-bearing horizons: Taskuduksky and Dzhilandinsky, confined to areas complicated by discontinuous tectonics.

In order to select and substantiate sound mining technology and ensure the safety of mining operations in mines and quarries, as well as in the construction and operation of hydraulic engineering and other technical facilities interacting with the surrounding rock mass, it is necessary to diagnose the initial stress field of the rock mass [30]-[33].

The specificity of the task of studying the rock mass stress state is that, in principle, it is impossible to directly measure the stresses acting in a solid medium, whether it is a rock composing the mass or an artificial structure made of metal, concrete, etc. It is possible to assess them qualitatively and, most importantly for practice, quantitatively by the manifestation of stresses in various mechanical and geophysical processes – deformability, destruction, etc. [34], [35].

This research analyzes the mechanical properties of ores and rocks of the Zhilandy Group field in order to determine the natural stress state of the mass. This will help us to effectively solve geomechanical problems and optimize mining operations. Given the diverse geological conditions in the area, our research is of value to both the scientific community and practical applications in the mining industry.

2. Methods

One of the most universal methods for assessing the natural stress field is the method of hydraulic fracturing of rocks in a well. On the one hand, the use of hydraulic rock fracturing in a well is effective for a detailed study of stress fields in the zones of influence of underground and surface facilities. On the other hand, this method can be used to diagnose the stress state in deep wells and is one of the few methods for this purpose [36]-[39].

Based on the hydraulic test data, the lower horizontal stress component value is determined, from which the higher horizontal stress component value is calculated. In this case, the calculation uses the values of physical-mechanical rock mass properties at the site of the experiment. It is important to note that the material content of rocks characterizes a qualitative rather than quantitative idea of physical-mechanical properties [40], [41]. Without measuring the physical-mechanical rock mass properties at the experiment site, the results of measuring stresses using the hydraulic fracturing method will be very approximate [42].

The sites for monitoring the stresses acting in the mass, as well as the location of metering stations is chosen at the maximum possible distance from the zone of stope operations [43]. The construction of the metering station provides for at least three 76 mm diameter wells up to 12 m deep. Next, the surface of the well walls is surveyed. Preferably, a measuring probe is installed in the well end area and a hydraulic fracturing test is performed. The critical fluid pressure at the time of hydraulic fracturing and its stabilization pressure after the fluid supply is stopped are recorded. Stabilization pressure is recorded for 5 min. The injection pressure is reset to zero and the well wall loading process is repeated 2-3 times with recording in each case. The measuring probe is repositioned in the direction towards the wellhead and placed in two or three places along the length of the well with a step of 1.0-1.5 m. Hydraulic fracturing tests are performed at each installation location. Based on the hydraulic fracturing test parameters, the value of the minimal and the value of the maximal horizontal component of the acting stress are determined. The measuring probe is then removed from the well.

2.1. Determining physical-mechanical mine rock properties

2.1.1. Rock samples

Five rock probes are tested. Laboratory samples for testing of physical-mechanical properties are drilled from the supplied rock probes. Twelve tests (six tests in natural and six in water-saturated states) are conducted for each probe.

Table 1 contains: probe number, rock name, sampling location, numbers of laboratory samples drilled from this probe and corresponding types of tests performed on these samples in natural and water-saturated states.

Table 1. Probe number, sampling location, types of tests and the corresponding sample numbers

Probe No.	Rock name	Sampling location	Sample numbers, types of tests, state			
			Compression		Tension	
			natural	water-saturated	natural	water-saturated
I	Ore grey sandstone	Ore (East Saryoba, P-6, deposit I-II, hor. 300 m, MCC)	1-1-1n, 1-1-2n, 1-1-3n, 1-1-4n, 1-1-5n, 1-1-6n	1-1-1w, 1-1-2w, 1-1-3w, 1-1-4w, 1-1-5w, 1-1-6w	1-2-1n, 1-2-2n, 1-2-3n, 1-2-4n, 1-2-5n, 1-2-6n	1-2-1w, 1-2-2w, 1-2-3w, 1-2-4w, 1-2-5w, 1-2-6w
II	Ore (Itauz field)	Ore (Itauz, 270 m sub-level incline)	2-1-1n, 2-1-2n, 2-1-3n, 2-1-4n, 2-1-5n, 2-1-6n	2-1-1w, 2-1-2w, 2-1-3w, 2-1-4w, 2-1-5w, 2-1-6w	2-2-1n, 2-2-2n, 2-2-3n, 2-2-4n, 2-2-5n, 2-2-6n	2-2-1w, 2-2-2w, 2-2-3w, 2-2-4w, 2-2-5w, 2-2-6w
III	Grey barren sandstone	Grey sandstone (East Saryoba, P-5, hor. 200 m, hanging block)	3-1-1n, 3-1-2n, 3-1-3n, 3-1-4n, 3-1-5n, 3-1-6n	3-1-1w, 3-1-2w, 3-1-3w, 3-1-4w, 3-1-5w, 3-1-6w	3-2-1n, 3-2-2n, 3-2-3n, 3-2-4n, 3-2-5n, 3-2-6n	3-2-1w, 3-2-2w, 3-2-3w, 3-2-4w, 3-2-5w, 3-2-6w
IV	Red sandstone	Red sandstone (East Saryoba, drift 3 west, hor. 100 m); Red sandstone (Itauz, 270 m sub-level)	4-1-1n, 4-1-2n, 4-1-3n, 4-1-4n, 4-1-5n, 4-1-6n	4-1-1w, 4-1-2w, 4-1-3w, 4-1-4w, 4-1-5w, 4-1-6w	4-2-1n, 4-2-2n, 4-2-3n, 4-2-4n, 4-2-5n, 4-2-6n	4-2-1w, 4-2-2w, 4-2-3w, 4-2-4w, 4-2-5w, 4-2-6w
V	Siltstone	Grey siltstone (North Karashoshak quarry); Sandy siltstone (North Karashoshak quarry)	1-1-1n, 1-1-2n, 1-1-3n, 1-1-4n, 1-1-5n, 1-1-6n	1-1-1w, 1-1-2w, 1-1-3w, 1-1-4w, 1-1-5w, 1-1-6w	1-2-1n, 1-2-2n, 1-2-3n, 1-2-4n, 1-2-5n, 1-2-6n	1-2-1w, 1-2-2w, 1-2-3w, 1-2-4w, 1-2-5w, 1-2-6w

The sampling technology ensures maximum preservation of the representativeness of the ore or rock in the probe in terms of composition, structure and condition. Monoliths suitable for core drilling are used as probes. The number and size of probes are determined depending on the number of lithological varieties, the type of tests to be performed and the number of samples made from probes to be tested (taking into account the repetition of tests to determine the coefficients of variation of indicators characterizing rock heterogeneity).

When selecting the sampling location, we strived for maximum typicality of the probes taken, namely to their correspondence in structure and properties to the rocks in the locations for which the assigned tasks are performed. At least two locations are sampled in each preparatory working and/or in the stoping face.

Probes are placed in sealed containers or in bags made of airtight materials. When using plastic bags, each probe is packed in a double bag. Each plastic bag is hermetically sealed. The air is removed from the bag before it is sealed. The bag with probe contains a sheet of paper with information on the date and time of sampling, the place of sampling, the natural ore type from which the probe is taken.

Deformation and strength properties of ore and host rock samples from Zhilandy field are tested using certified equipment. A general view of the complex for testing core samples is shown in Figure 2.

Figure 2. Core sample testing complex based on a Servo Hydraulic Press Machine INSTRON 8802

For testing, ore and host rock samples are taken with the following parameters: diameter – at least 30 ± 1 mm, height – 60 ± 2 mm, and at least 3 pieces of each type of samples.

The minimum dimensions of ore pieces suitable as a probe for mechanical testing are for monoliths of at least 200×200×150 mm, excluding areas disturbed during separation from the mass. The core samples in the Zhilandy field were taken under these conditions.

The press provides the modes of soft (loading program is set on loads, to identify the tendency of rocks to brittle fracture and rock-bump hazard) and hard (loading program is set on moving the gripper) loading with automatic recording of measurement results in the computer memory. During the experiments the axial load, longitudinal and transverse deformations in the middle part of the sample (25 mm base) are continuously measured and recorded using INSTRON strain gauges, as well as the value of the press traverse displacement. For volumetric compression tests, an additional recording is made of the lateral pressure applied to the sample placed in the compression chamber. The equipment meets the requirements of international standards and helps to obtain strength, deformation characteristics at all stages of loading the samples, including post-peak, up to their destruction.

The diameter (d) of the core samples is at least 30 mm, the ratio of height (L) to diameter (shape factor L/d) is: 0.5-1 in the tension testing; 2.0 – in the compression testing. Samples are prepared using special equipment for core processing – a system for high-precision manufacturing of cylinders and end surfaces of cores manufactured by Coretest Systems, USA. The deviation from parallelism of the end surfaces of the test samples is not more than 0.05 mm by the sample base diameter; deviation from the perpendicularity of the ends to the cylinder generatrix is no more than 0.05 mm; end convexity – less than 0.003 mm according to the requirements of GOST 28985-91.

2.1.2. Determining the ultimate strength for uniaxial compression

The uniaxial compression strength of rocks is determined according to GOST 21153.2-84. Cylindrical samples of 30 mm diameter with a height (h) ratio to its diameter (d) equal to $m = h/d = 2.0$ are used for the tests. The sample diameters are measured in three places in its height (in the middle and at the ends). The arithmetic mean of the results of all measurements is taken as the nominal diameter. Measurements are made using a digital caliper with an error of ±0.001 mm.

The samples are loaded during testing at a movement velocity of 0.1 mm/min of the press movable traverse. The ultimate strength value for uniaxial compression σ_c (MPa) is calculated by the Formula:

$$\sigma_c^o = \frac{P_{\max}}{S}, \quad (1)$$

where:

P_{max} – maximum destructive load;

S – sample cross-sectional area.

2.1.3. Determining deformation characteristics in uniaxial compression

The deformation properties of rocks are studied in accordance with GOST 28985-91. This normative document is applicable to hard rocks with ultimate strength for uniaxial compression of at least 5 MPa and determines the method for measuring their deformation parameters.

To conduct an experiment on determining the mechanical sample properties, longitudinal (ε_1) and transverse (ε_2) deformations, as well as axial load (P) have been recorded using a measuring complex that operates automatically throughout the loading process until the sample destruction. The measurement frequency is 10 Hz.

The stress is calculated from the Expression:

$$\sigma = \frac{4P}{\pi d^2}. \quad (2)$$

Young's modulus E and Poisson's ratio ν are determined according to GOST 28985-9 in the selected stress range $\sigma_b - \sigma_e$ of the load branch straight section using the following Formulas:

$$E = \frac{\sigma_e - \sigma_b}{\varepsilon_{1e} - \varepsilon_{1b}}, \quad \nu = \frac{\varepsilon_{2f} - \varepsilon_{2i}}{\varepsilon_{1e} - \varepsilon_{1b}}, \quad (3)$$

where:

σ_e – the stress level values at the end of the range under load, MPa;

σ_b – the stress level values at the beginning of the range under load, MPa;

ε_{1b} – the relative longitudinal stresses of the material at the beginning of the range under load;

ε_{1e} – the relative longitudinal stresses of the material at the end of the range under load;

ε_{2i} – the transverse sample deformations measured relative to the initial load value within the specified range.

ε_{2f} – are the transverse sample deformations measured relative to the final load value within the specified range.

In the case of nonlinear stress-strain dependence, the linear approximation method is used.

2.1.4. Determining deformation characteristics in uniaxial tension

The ultimate tensile strength of rocks (Brazilian test) is determined according to GOST 21153.3-85. The standard is applicable to rocks with an ultimate strength for uniaxial tension of not less than 0.5 MPa. The prepared cylindrical samples with a diameter of 30 mm meet the requirements of clause 1.3.4 and clause 2.3.4 of GOST 21153.3-85.

The ultimate strength in indirect tension is determined by the method of destruction of cylindrical samples by compression along the generatrixes. During testing, the sample is placed in the center of the support plate of the testing machine (press) between spacer plates. The sample is loaded uniformly at a velocity of 0.1 mm/min until its destruction. The value of the destructive force (P) is fixed by the force meter of the testing machine. The ultimate tensile strength (σ_t) is calculated using the Formula:

$$\sigma_t = 0.64 \cdot \frac{P}{S}, \quad (4)$$

where:

P – the sample destructive force;

S – the area of the sample rupture, equal to the product of the sample diameter (d) by its length (L).

2.1.5. Determining rock density and moisture content

The rock moisture content in the natural state is determined in accordance with GOST 8269.0-97. A VIBRA AF-R220CE drying cabinet and scales are used for this research.

To determine the density of rock samples in the natural state (ρ_n), the samples are weighed, the mass (m_n) is determined, and the diameter (D) and length (L) of the samples are measured. Density is determined by the Formula:

$$\rho_n = \frac{m_n}{V};\ V = \pi \cdot L \cdot \frac{D^2}{4}, \quad (5)$$

where:

m_e – the sample mass in its natural state;

V – is the sample volume.

To determine water absorption, five samples of each probe, dried to constant mass, are placed in a vessel with water so that the water level is above the top surface of the samples by at least 20 mm. The samples are held in this condition for 48 hours, and then they are removed from the vessel and weighed. Water absorption can be determined by the Formula:

$$W_n = \frac{m_n - m_d}{m_d} \cdot 100\%, \quad (6)$$

where:

m_e – the sample mass in its natural state;

m_d – the mass of the sample dried to constant mass.

2.2. Instruments for performing experiments in mine conditions

The set of equipment for conducting experimental tests in mine conditions includes: measuring-computing complex "Hydraulic fracturing", a downhole video probe for surveying measuring wells, as well as devices for cutting annular and longitudinal slots on the well walls (Fig. 3). The "Hydraulic fracturing" measuring-computing complex includes: two-packer probe, hand pump, pressure gauge, pressure pipelines, switching equipment, as well as a pressure recording system consisting of a pressure gauge with pressure sensor, personal computer, connecting cables and charger. This set of equipment is portable and designed for use in underground environments. In the underground environment, the pressure meter wirelessly transmits the experimental data to a personal computer, in which they are stored and automatically processed.

Figure 3. Equipment for measuring the natural stress field at the metering station

In-situ experiments use measuring probes of two designs. The measuring probe, equipped with four packers (Fig. 4), has two hydraulic cylinders that are used to axially compress the packer elements. When conducting research, there is a possibility to change the size of the inter-packer space by replacing the central segment of the bearing rod. When conducting hydraulic fracturing during testing, the size of the interpacker space is 5-6 diameters. The measuring probe is equipped with guiding plates for ease of setting the device into a 76 mm diameter measuring well. Figure 5 shows the view of a measuring probe equipped with four polyurethane packers. The probe also comprises guiding plates, hydraulic cylinders and a sleeve for filling the interpacker space.

In a two-packer probe (Fig. 5), axial compression of the packer elements is performed using a hydraulic cylinder located in the central part. The construction provides for the use of packing elements reinforced with springs.

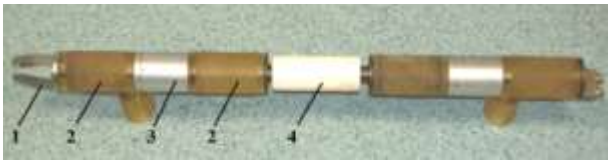

Figure 4. General view of the measuring probe with four packers: 1 – guiding plates; 2 – polyurethane sealing packers; 3 – hydraulic cylinders; 4 – spacer sleeve for filling the interpacker space

Figure 5. General view of the two-packer measuring probe: 1 – polyurethane packers with springs; 2 – hydraulic cylinder; 3 – spacer sleeve; 4 – guiding plates

3. Results and discussion

As a result of a series of experimental studies, the results of laboratory tests aimed at determining the deformation and strength characteristics of rock samples are presented below. The main results are graphically presented (Figs. 6-12) and analyzed in Tables 2-7.

Figure 6 shows the results of probe density determination at natural moisture content (ρ). Probe density values range from 2521 to 2707 kg/m³.

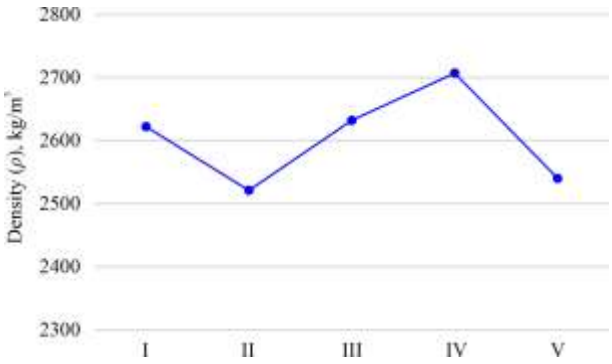

Figure 6. Averaged densities of probes at natural moisture content (ρ), kg/m³

Figure 7 shows the averaged ultimate strengths of probes for uniaxial compression (σ_c) in natural and water-saturated states.

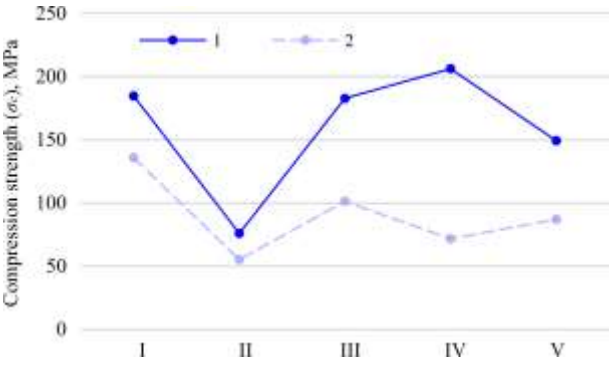

Figure 7. Averaged ultimate strengths of probes for uniaxial compression (σ_c), MPa: 1 – in natural state; 2 – in water-saturated state

To analyze the data provided, compare the average ultimate strength of probes for uniaxial compression (σ_c^e) in natural state and water-saturated state (σ_c^w) for each of the probes (Table 2).

All probes show a decrease in ultimate strength for uniaxial compression under water saturation. This indicates that water saturation significantly weakens the rocks. Probe IV shows the most significant decrease in ultimate strength: from 206.3 to 71.7 MPa, which is 134.6 MPa or 65.2%.

Table 2. Comparison of probe ultimate strength for uniaxial compression data (σ_c)

Parameter studied	I	II	III	IV	V
Average ultimate strength of probes for uniaxial compression in their natural state (σ_c^n), MPa	184.7	76.0	182.8	206.3	149.3
Average ultimate strength of probes for uniaxial compression in their water-saturated state (σ_c^w), MPa	135.9	55.3	101.3	71.7	87.1
Differential (Δ), MPa	48.8	20.7	81.5	134.6	62.2
Percentage change (Δ), %	-26.4	-27.2	-44.6	-65.2	-41.6

Probe I has the smallest decrease in absolute values: from 184.7 to 135.9 MPa, which is 48.8 MPa or 26.4%. Thus, there is a significant decrease in ultimate strength under water saturation in all the probes presented. The most vulnerable to water saturation is probe IV, which loses more than 65% of its strength. Probe I is the least vulnerable to water saturation, losing about 26% of its strength.

Figure 8 presents the averaged ultimate strengths of probes for uniaxial tension (σ_t) in natural and water-saturated states.

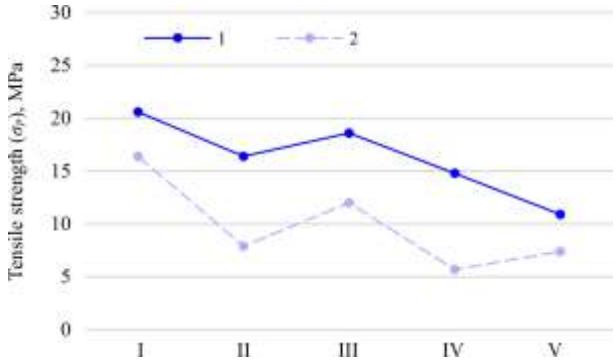

Figure 8. Averaged ultimate strengths of probes for uniaxial tension (σ_t), MPa: 1 – in natural state; 2 – in water-saturated state

To analyze the data provided, compare the average ultimate strength of probes for uniaxial tension (σ_t^e) in natural state and water-saturated state (σ_t^w) for each of the probes (Table 3).

Table 3. Comparison of probe ultimate strength for uniaxial tension data (σ_t)

Parameter studied	I	II	III	IV	V
Average ultimate strength of probes for uniaxial tension in their natural state (σ_t^n), MPa	20.6	16.4	18.6	14.8	10.9
Average ultimate strength of probes for uniaxial tension in their water-saturated state (σ_t^w), MPa	16.4	7.9	12.0	5.7	7.4
Differential (Δ), MPa	4.2	8.5	6.6	9.1	3.5
Percentage change (Δ), %	-20.3	-51.8	-35.4	-61.4	-32.1

Similar to uniaxial compression, all probes show a decrease in ultimate tensile strength under water saturation. Probe IV shows the most significant decrease in ultimate strength: from 14.8 to 5.7 MPa, which is 9.1 or 61.49%.

Probe V has the smallest decrease in absolute values: from 10.9 to 7.4 MPa, which is 3.5 MPa or 32.11%. Accordingly, all probes show a significant decrease in ultimate tensile strength under water saturation. The largest decrease, both in absolute and percentage values, is observed in probe IV, confirming its high vulnerability to water saturation. The smallest decrease is in probe I, indicating its relative water resistance.

Figure 9 shows the averaged Young's moduli (E) of probes in natural and water-saturated states.

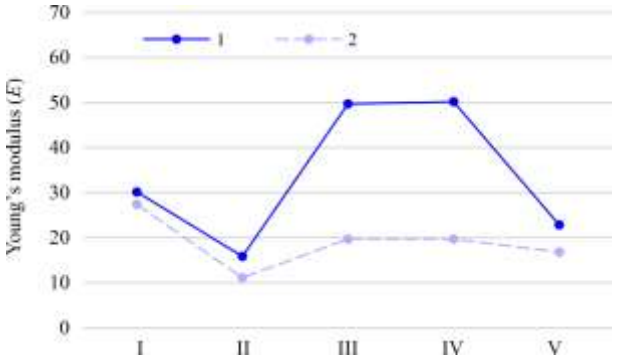

Figure 9. Averaged Young's moduli of probes (E), GPa: 1 – in natural state; 2 – in water-saturated state

To analyze the data provided, compare the averaged Young's moduli of probes in natural state (E^n) and water-saturated state (E^w) for each of the probes (Table 4).

Table 4. Comparison of probe Young's modulus data (E)

Parameter studied	I	II	III	IV	V
Average Young's modulus of probes in natural state (E^n), GPa	30.1	15.8	49.7	50.1	22.8
Average Young's modulus of probes in water-saturated state (E^w), GPa	27.3	11.1	19.6	19.6	16.8
Differential (Δ), GPa	2.7	4.7	30.0	30.4	6.0
Percentage change (Δ), %	-9.1	-29.7	-60.3	-60.7	-26.2

All probes show a decrease in Young's modulus under water saturation. Probes III and IV show the most significant decrease in Young's modulus: probe III – from 49.7 to 19.6 GPa, which is 30.0 GPa or 60.37%, probe IV – from 50.1 to 19.6 GPa, which is 30.4 or 60.7%. Probe I has the smallest decrease in absolute values: from 30.1 to 27.3 GPa, which is 2.7 GPa or 9.1%. Consequently, all probes show a decrease in Young's modulus during water saturation, indicating a decrease in the hardness of the material influenced by water. The largest decrease is observed for probes III and IV, which lose more than 60% of their hardness. The smallest decrease is in probe I, indicating its relative water resistance.

Figure 10 shows the averaged Poisson's ratios of probes (v) in natural and water-saturated states.

To analyze the data provided, compare the averaged Poisson's ratios of probes in natural state (v^n) and water-saturated state (v^w) for each of the probes (Table 5).

In most probes, Poisson's ratio increases under water saturation, except for probe III, which shows a slight decrease. Probe IV shows the largest increase in Poisson's ratio: from 0.159 to 0.187, which is 0.028 or 17.61%.

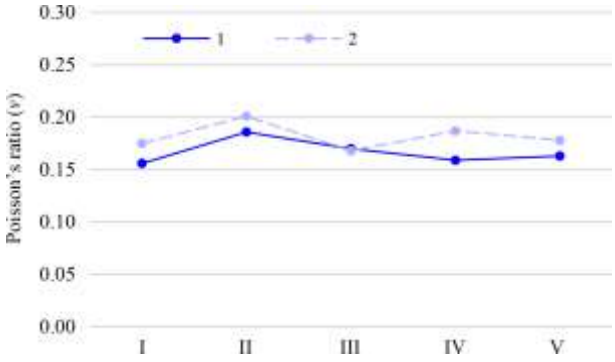

Figure 10. Averaged Poisson's ratios of probes (v): 1 – in natural state; 2 – in water-saturated state

Table 5. Comparison of probe Poisson's ratio data (v)

Parameter studied	I	II	III	IV	V
Average Poisson's ratio of probes in natural state (v^n)	0.156	0.186	0.170	0.159	0.163
Average Poisson's ratio of probes in water-saturated state (v^w)	0.175	0.201	0.166	0.187	0.178
Differential (Δ)	0.019	0.015	-0.002	0.028	0.015
Percentage change (Δ), %	12.18	8.06	-1.18	17.61	9.20

All probes, except for probe III, show an increase in Poisson's ratio under water saturation, indicating an increase in the material flexibility in the transverse direction under the influence of water. The largest increase in Poisson's ratio is observed in probe IV, indicating its high vulnerability to water saturation.

Figure 11 shows the averaged cohesion factors of probes (c) in natural and water-saturated states.

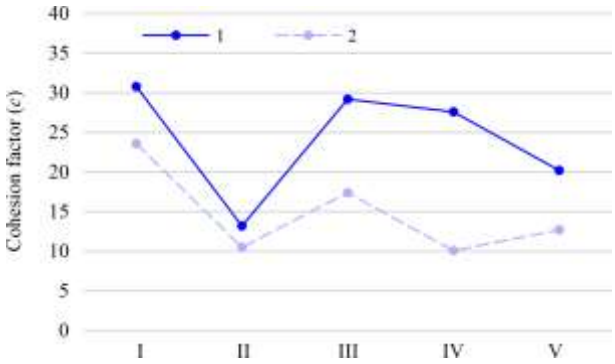

Figure 11. Averaged cohesion factors of probes (c): 1 – in natural state; 2 – in water-saturated state

To analyze the data provided, compare the averaged cohesion factors of probes in natural state (c^n) and water-saturated state (c^w) for each of the probes (Table 6).

Table 6. Comparison of probe cohesion factor data (c)

Parameter studied	I	II	III	IV	V
Average cohesion factor of probes in natural state (c^n)	30.8	13.2	29.2	27.6	20.2
Average cohesion factor of probes in water-saturated state (c^w)	23.6	10.5	17.4	10.1	12.7
Differential (Δ)	7.2	2.7	11.8	17.5	7.5
Percentage change (Δ), %	-23.3	-20.45	-40.41	-63.41	-37.13

All probes show a decrease in cohesion factor under water saturation. Probe IV shows the most significant decrease in cohesion factor: from 27.6 to 10.1 MPa, which is 17.5 MPa or 63.41%. Probe II has the smallest decrease in absolute values: from 13.2 to 10.5 MPa, which is 2.7 or 20.45%. Thus, in all probes there is a significant decrease in cohesion factor under water saturation. The largest decrease, both in absolute and percentage values, is observed for probe IV, confirming its high vulnerability to water saturation. Probe II has the smallest decrease, indicating its relative resistance to water.

Figure 12 shows the averaged internal friction angles (φ) in natural and water-saturated states.

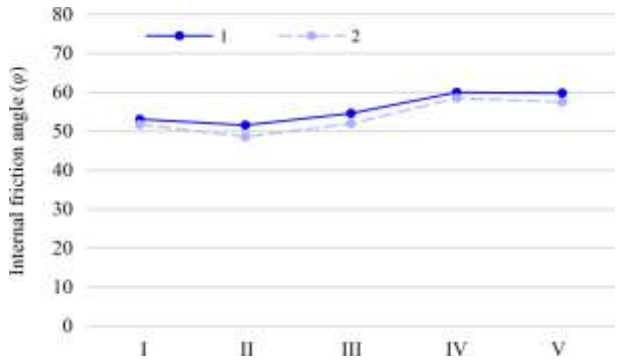

Figure 12. Averaged internal friction angles of probes (φ): 1 – in natural state; 2 – in water-saturated state

To analyze the data provided, compare the averaged internal friction angles of probes in natural state (φ^n) and water-saturated state (φ^w) for each of the probes (Table 7).

Table 7. Comparison of probe internal friction angle data (φ)

Parameter studied	I	II	III	IV	V
Average internal friction angle of probes in natural state (φ^n), deg	53.1	51.6	54.6	60.0	59.8
Average internal friction angle of probes in water-saturated state (φ^w), deg	51.7	48.6	52.0	58.5	57.5
Differential (Δ), deg	1.4	3.0	2.6	1.5	2.3
Percentage change (Δ), %	-2.6	-6.1	-5.0	-2,5	-3.8

In most probes, the average internal friction angle decreases under water saturation. Probes II and IV show the greatest decrease in internal friction angle: probe II from 51.6 to 48.6°, and probe IV from 60.0 to 58.5°. Probe I shows the smallest decrease in the internal friction angle: from 53.1 to 51.7°. Consequently, the average internal friction angle decreases in most probes under water saturation, indicating a decrease in the cohesion between the material particles. The greatest decrease in the internal friction angle is observed in probes II and IV, indicating a stronger erosion of the material by water and deterioration in its ability to resist shear stresses.

Based on the results of reduced geomechanical core documentation of exploration work in the Itauz field, the data on mass fracture disturbance have been processed. The rocks in the field vary from moderately fractured to massive, with an average RQD of about 70-80% (Fig. 13).

During the drilling of wells to measure the natural field, cores from these wells have been documented. Based on the core documentation results, the mass quality in this area is quite stable.

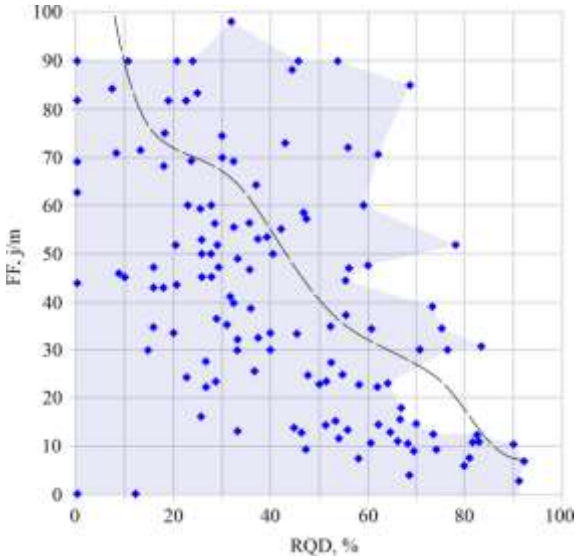

Figure 13. Dependence of RQD on FF based on data from all wells in the Itauz field

At the same time, many mechanical fractures are observed, formed as a result of drilling and during core transportation. Core destruction is observed at the beginning of the well, indicating low-quality drilling and blasting operations and stresses on the mine working contour.

A total of about 280 measurements of rock mass fracturing using linear mapping have been made at the Itauz mine. An example of an image of rock mass fracturing in the Itauz field is presented in Figure 14.

Figure 14. Image of the Itauz field rock mass fracturing

Based on the data presented, it can be concluded that the rock mass presented in the research has a conditionally average to good RQD (Rock Quality Designation) quality. RQD is an index used to assess the rock mass quality based on the number of fractures and their distribution in rock samples.

The stability of rocks is highly dependent on the characteristics of fractures, such as their filling and microroughness. Filling of fractures can influence the permeability of rocks and their resistance to water, which in turn influences their strength under water saturation. Microroughness, or fine roughness of fracture surface, is also important because it can enhance the rock fracture resistance and reduce the probability of destruction under mechanical loading. Analysis of the characteristics of fractures in rocks leads to the conclusion about their stability.

The rock mass is characterized by irregular fracturing. It is of tectonic origin and for different lithological varieties, the average is: for the Itauz field – 10-15 fractures per meter.

Examples of polar fracture diagrams of the rock mass around incline No. 5 (270 m sub-level) and the rock mass around the mine working (290 m sub-level) of the Itauz field are presented in Figure 15. To determine the formation of wedge-shaped inrushes in the mine working roof depending on the azimuth of its drifting and fracturing, numerical modeling in Unwedge software is performed. Direct measurements have determined that there are three to four fracture systems in the field (Fig. 16).

Thus, based on the modeling results, critical directions of the existing fracture systems have been determined, along which maximum wedges are formed, that is, directions of drifting in these azimuths will be accompanied by the risk of large wedge-shaped failures.

(a)

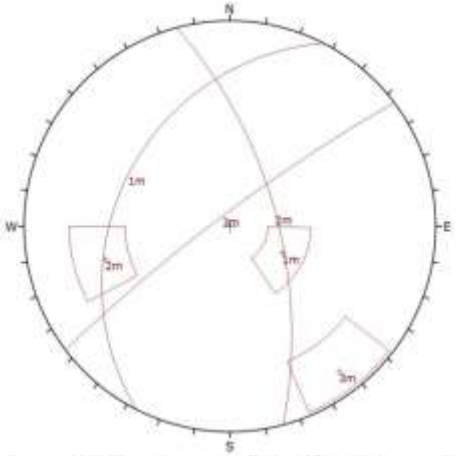

	Color	Dip	Dip Direction	Label
Mean Set Planes				
1m		32	117	
2m		64	255	
3m		83	143	

Plot Mode	Pole Vectors
Vector Count	30 (30 Entries)
Hemisphere	Upper
Projection	Equal Angle

Color	Density Concentrations
	0.00 - 2.20
	2.20 - 4.40
	4.40 - 6.60
	6.60 - 8.80
	8.80 - 11.00
	11.00 - 13.20
	13.20 - 15.40
	15.40 - 17.60
	17.60 - 19.80
	19.80 - 22.00

Contour Data	Pole Vectors
Maximum Density	21.51%
Contour Distribution	Fisher
Counting Circle Size	1.0%

Plot Mode	Pole Vectors
Vector Count	30 (30 Entries)
Hemisphere	Upper
Projection	Equal Angle

(b)

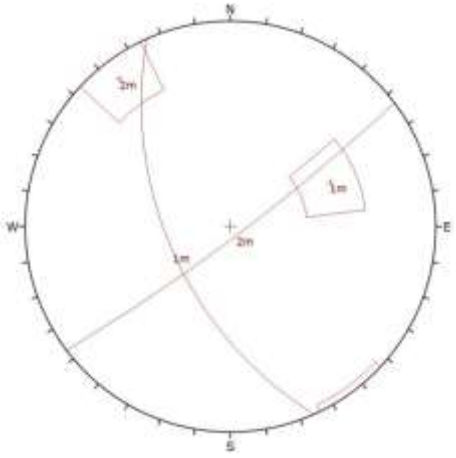

	Color	Dip	Dip Direction	Label
Mean Set Planes				
1m		56	66	
2m		84	323	

Plot Mode	Pole Vectors
Vector Count	30 (30 Entries)
Hemisphere	Upper
Projection	Equal Angle

Color	Density Concentrations
	0.00 - 3.20
	3.20 - 6.40
	6.40 - 9.60
	9.60 - 12.80
	12.80 - 16.00
	16.00 - 19.20
	19.20 - 22.40
	22.40 - 25.60
	25.60 - 28.80
	28.80 - 32.00

Contour Data	Pole Vectors
Maximum Density	31.92%
Contour Distribution	Fisher
Counting Circle Size	1.0%

Plot Mode	Pole Vectors
Vector Count	30 (30 Entries)
Hemisphere	Upper
Projection	Equal Angle

Figure 15. Fracture diagrams of the rock mass in the Itauz field: (a) 270 m sub-level; (b) 290 m sub-level

(a)

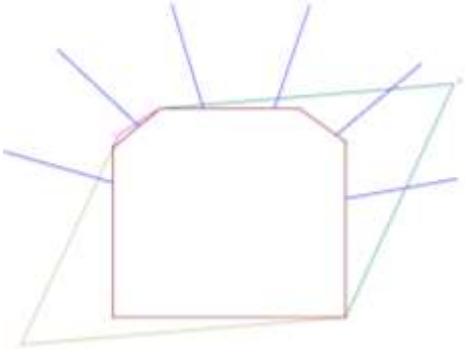

(b)

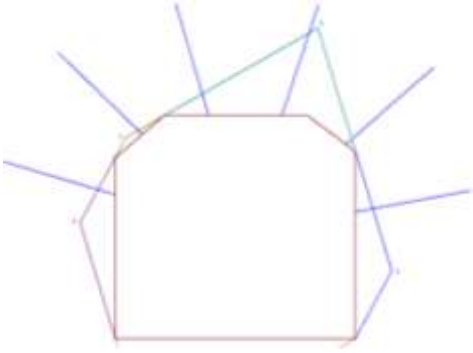

Figure 16. Wedges at different azimuths of mine working drifting: (a)120°; (b) 141°

Based on the results of measuring the natural stress field within the Zhilandy Group field, the Trust Faulting tectonic mode has been revealed, namely tectonic maximum, minimum and vertical stresses ($\sigma_1 > \sigma_2 > \sigma_v$). Dependence of stress with depth based on measurement results is presen-ted in Figure 17.

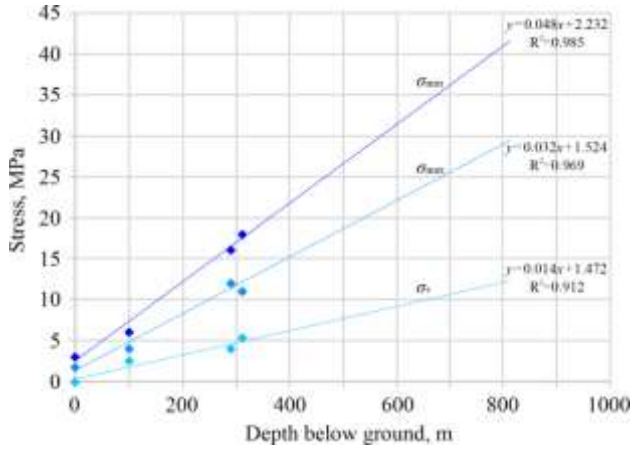

Figure 17. Linear dependences of stress variation with depth based on measurement results

According to the RQD and FF quality data, the mass ranges from moderately fractured to massive with localized zones of crushing and fault. Based on the results of the fracture survey, unfavorable directions for the sites have been identified. For subsequent drifting, it is recommended to locate the mine workings (by the geological and geomechanical service of the mine) for kinematic analysis of the mine working stability and roof control. The stability of mine workings is mainly influenced by fracture filler and fracture micro-roughness, which requires more detailed study, since when documenting the core of wells for hydraulic fracturing, fracture filler is represented by carbonate.

The lithostatic pressure ($\sigma_h = \gamma h$) for metering station No. 1 at 123.5 m mark is about 9.0 MPa. Having performed 17 hydraulic fracturing tests at metering station No. 1 and as a result of processing $p - t$ diagrams, the following values of stresses acting in the mass have been found:

– σ_{min} = 10.55-11.68 MPa ≈ 1.2 γh;

– σ_{max} = 18.36-20.76 MPa ≈ 2.14 γh;

– σ_v = 9.12 MPa.

The direction of maximum horizontal stress is oriented along an azimuth of 70°±10. The value of σ_v is taken as γh (σ_v may be different from γh due to overmining or undermining of the mass). These measurements can be considered as a natural stress field at a given depth (distance from the surface is about 310 m).

Lithostatic pressure ($\sigma_h = \gamma h$) for metering station No. 2 at 42 m mark is about 8.5 MPa. Having performed 18 hydraulic fracturing tests at metering station No. 2 and as a result of processing $p - t$ diagrams, the following values of stresses acting in the mass have been found:

– σ_{min} = 11.63-13.5 MPa ≈ 1.35-1.56 γh;

– σ_{max} = 15.0-17.2 MPa ≈ 1.74-2.0 γh;

– σ_v = 8.08-9.0 MPa.

The direction of maximum horizontal stress is oriented along an azimuth of 70°±10. The average value of the obtained σ_v = 8.61 MPa is taken as γh.

A total of 35 hydraulic fracturing tests have been performed at two metering stations. It has been determined that there is tectonic stress in the field, which may be due to the shape of structural folds and tectonic fracturing. The azimuth of the maximum horizontal stress action at the studied stations coincides and is equal to 70°±10.

4. Conclusions

The research results of mechanical properties of materials in natural and water-saturated states lead to the following general conclusions:

– all test materials show a decrease in ultimate strength for compression, tension and shear under water saturation, indicating that water saturation has a negative influence on the strength of materials;

– water saturation also leads to a decrease in the Young's modulus of materials, indicating that their hardness decreases under the influence of water;

– under the influence of water saturation, the Poisson's ratio and internal friction angle of materials also change, which may influence their ability to deform and cohesion between particles;

– water saturation leads to a decrease in the cohesion coefficient of materials, which may influence their ability to resist shear stresses and resistance to various loads.

Thus, it is important to emphasize the importance of taking water saturation into account when assessing the natural field of mass stress state. Such data make it possible to more accurately predict the behavior of the rock mass under different conditions and informed decision-making when designing and operating mine workings.

It has been revealed that the rock mass is characterized by non-uniform fracturing. It is of tectonic origin and averages between 10-15 and 15-25 fractures per meter for different lithological varieties.

To determine the formation of wedge-shaped inrushes in the mine working roof depending on the azimuth of its drifting and fracturing, numerical modeling in Unwedge software is performed. Direct measurements have determined that there are three to four fracture systems in the field. Based on the modeling results, critical directions of the existing fracture systems have been determined, along which maximum wedges are formed, that is, directions of drifting in these azimuths will be accompanied by the risk of large wedge-shaped failures. The azimuths of the direction of mine workings with the largest and the smallest inrush volumes have been determined.

A total of 35 hydraulic fracturing tests have been conducted at two metering stations, revealing the stress parameters in the rock mass. For metering station No. 1 at 123.5 m depth, the lithostatic pressure is about 9.0 MPa, with minimum horizontal stress ranging from 10.55 to 11.68 MPa, maximum horizontal stress ranging from 18.36 to 20.76 MPa, and vertical stress equal to 9.12 MPa. For metering station No. 2 at 42 m depth, the lithostatic pressure is about 8.5 MPa, the minimum horizontal stress ranges from 11.63 to 13.5 MPa, the maximum horizontal stress ranges from 15.0 to 17.2 MPa, and the vertical stress ranges from 8.08 to 9.0 MPa. The maximum horizontal stress at both stations is oriented along an azimuth of 70° ± 10. In general, the data indicate that there is tectonic stress in the mass, which may be due to the shape of structural folds and tectonic fracturing.

Author contributions

Conceptualization: AM, NS; Data curation: SZ, RI; Formal analysis: AM, AK; Funding acquisition: RM; Investigation: NS; Methodology: RI; Project administration: RM, AK; Resources: AM, DD; Software: SZ, RI; Supervision: AM, RI; Validation: SZ, NS; Visualization: SZ, DD; Writing – original draft: AM, DD, RI; Writing – review & editing: AM, NS, AK. All authors have read and agreed to the published version of the manuscript.

Funding

This research has been funded by the Science Committee of the Ministry of Science and Higher Education of the Republic of Kazakhstan (Grant No. AP14972815).

Acknowledgements

The authors thank the editor and the anonymous reviewers for reviewing an earlier version of this manuscript and offering valuable suggestions.

Conflicts of interests

The authors declare no conflict of interest.

Data availability statement

The original contributions presented in the study are included in the article, further inquiries can be directed to the corresponding author.

References

[1] Yessengeldin, B., Khussainova, Z., Kurmanova, A., Syzdykova, D., & Zhanseitov, A. (2019). Exploitation of Natural Resources in Kazakhstan: Judicial Practice for Foreign Investment. *Journal of East Asia and International Law*, *12*(1), 169-179. https://doi.org/10.14330/jeail.2019.12.1.09

[2] Smith, D.R. (2019). Kazakhstan. *Environmental Resources and Constraints in the Former Soviet Republics*, 251-274. https://doi.org/10.4324/9780429037344-16

[3] Atakhanova, Z., & Azhibay, S. (2023). Assessing economic sustainability of mining in Kazakhstan. *Mineral Economics*, *36*(4), 719-731. https://doi.org/10.1007/s13563-023-00387-x

[4] Chlachula, J. (2020). Geoheritage of East Kazakhstan. *Geoheritage*, *12*(4), 91. https://doi.org/10.1007/s12371-020-00514-y

[5] Mendygaliyev, A., Arshamov, Y., Selezneva, V., Yazikov, E., & Bekbotayeva, A. (2021). Prospects for application of multi-spectral earth sensing data in forecasting and searching for reservoir-infiltration uranium deposits. *News of the National Academy of Sciences of the Republic of Kazakhstan, Series of Geology and Technical Sciences*, *2*(446), 90-97. https://doi.org/10.32014/2021.2518-170x.39

[6] Seitmuratova, E., Arshamov, Y., Bekbotayeva, A., Baratov, R., & Dautbekov, D. (2016). Priority metallogenic aspects of late paleozioc volcanic-plutonic belts of Zhongar-Balkhash fold system. *International Multidisciplinary Scientific GeoConference Surveying Geology and Mining Ecology Management*, *1*, 511-518. https://doi.org/10.5593/sgem2016/b11/s01.064

[7] Issatayeva, F.M., Rudko, G.I., & Portnov, V.S. (2019). Technical and economic substantiation of developing Kusmuryn copper deposit (Kazakhstan). *Naukovyi Visnyk Natsionalnoho Hirnychoho Universytetu*, *6*, 19-24. https://doi.org/10.29202/nvngu/2019-6/3

[8] Mambetaliyeva, A.R., Mamyrbayeva, K.K., Turysbekov, D.K., Dauletbakov, T.S., & Barmenshinova, M.B. (2022). Investigation of the process of sulfiding of gold-arsenic containing ores and concentrates. *Naukovyi Visnyk Natsionalnoho Hirnychoho Universytetu*, *3*, 51-56. https://doi.org/10.33271/nvngu/2022-3/051

[9] Rysbekov, K.B., Bitimbayev, M.Z., Akhmetkanov, D.K., & Miletenko, N.A. (2022). Improvement and systematization of principles and process flows in mineral mining in the Republic of Kazakhstan. *Eurasian Mining*, *1*, 41-45. https://doi.org/10.17580/em.2022.01.08

[10] Kirsanov, A.K., Volkov, E.P., Kurchin, G.S., Shkaruba, N.A., Nafikov, R.Z., & Teshaev, U.R. (2022). The Central Asian states' role in the world mining industry. *Journal of Degraded & Mining Lands Management*, *9*(3), 3431–3443. https://doi.org/10.15243/jdmlm.2022.093.3431

[11] Zainal, P., Zhakupova, S., & Iztayeva, A. (2019). Analysis of inflow the direct foreign investments in priority sector the economy of Kazakhstan. *Farabi Journal of Social Sciences*, *5*(1), 54-63. https://doi.org/10.26577/CAJSH-2019-1-s7

[12] Fodor, M.M., Komorowski, M., & Turegeldinova, A. (2023). The relationship between firm attributes and attitudes towards diversity. *Sustainability*, *15*(9), 7481. https://doi.org/10.3390/su15097481

[13] Serikkaliyeva, A.E. (2016). Chinese investment in the mining and metallurgical complex of Kazakhstan. *Journal of Oriental Studies*, *78*(3), 58-61. https://doi.org/10.26577/JOS-2016-3-874

[14] Abuova, R.Zh., Ten, E.B., & Burshukova, G.A. (2021). Study of vibration properties of ceramic-metal nanostructural tin-cu coatings with different copper content 7 and 14 at. % on chromium-nickel-vanadium steels. *News of the National Academy of Sciences of the Republic of Kazakhstan, Series of Geology and Technical Sciences*, *5*(449), 6-13. https://doi.org/10.32014/2021.2518-170X.92

[15] Yelemessov, K., Krupnik, L., Bortebayev, S., Beisenov, B., Baskanbayeva, D., & Igbayeva, A. (2020). Polymer concrete and fibre concrete as efficient materials for manufacture of gear cases and pumps. *E3S Web of Conferences*, *168*, 00018. https://doi.org/10.1051/e3sconf/202016800018

[16] Khussan, B., Abdiev, A., Bitimbayev, M., Kuzmin, S., Issagulov, S., & Matayev, A. (2022). Substantiation and development of innovative container technology for rock mass lifting from deep open pits. *Mining of Mineral Deposits*, *16*(4), 87-95. https://doi.org/10.33271/mining16.04.087

[17] Yelemessov, K., Nauryzbayeva, D., Bortebayev, S., Baskanbayeva, D., & Chubenko, V. (2021). Efficiency of application of fiber concrete as a material for manufacturing bodies of centrifugal pumps. *E3S Web of Conferences*, *280*, 07007. https://doi.org/10.1051/e3sconf/202128007007

[18] Skidin, I.E., Vodennikova, O.S., Saithareiev, L.N., Baboshko, D.Y., & Barmenshinova, M.B. (2023). Technology of forming a wear-resistant thermite alloy layer based on the Fe-Cr-C system by self-propagating high-temperature synthesis. *IOP Conference Series: Earth and Environmental Science*, *1254*(1), 012008. https://doi.org/10.1088/1755-1315/1254/1/012008

[19] Sladkowski, A., Utegenova, A., Elemesov, K., & Stolpovskikh, I. (2017). Determining of the rational capacity of a bunker for cyclic-and-continuous technology in quarries. *Naukovyi Visnyk Natsionalnoho Hirnychoho Universytetu*, *6*, 29-33.

[20] Ivadilinova, D.T., Issabek, T.K., Takhanov, D.K., & Yeskenova, G.B. (2023). Predicting underground mining impact on the earth's surface. *Naukovyi Visnyk Natsionalnoho Hirnychoho Universytetu*, *1*, 32-37. https://doi.org/10.33271/nvngu/2023-1/032

[21] Arystan, I.D., Nemova, N.A., Baizbaev, M.B., & Mataev, A K. (2021). Efficiency of modified concrete in lining in underground structures. *IOP Conference Series. Earth and Environmental Science*, *77*, 012063. https://doi.org/10.1088/1755-1315/773/1/012063

[22] Pysmennyi, S., Chukharev, S., Peremetchy, A., Fedorenko, S., & Matsui, A. (2023). Study of stress concentration on the contour of underground mine workings. *Inżynieria Mineralna*, *1*(1(51)), 69-78. https://doi.org/10.29227/IM-2023-01-08

[23] Imashev, A.Zh., Sudarikov, A.E., Musin, A.A., Suimbayeva, A.M., & Asan, S.Yu. (2021). Improving the quality of blasting indicators by studying the natural stress field and the impact of the blast force on the rock mass. *News of the National Academy of Sciences of the Republic of Kazakhstan*, *4*(448), 30-35. https://doi.org/10.32014/2021.2518-170x.78

[24] Imansakipova, B.B., Baygurin, Z.D., Soltabaeva, S.T., Milev, I., & Miletenko, I.V. (2014). Causes of strain of buildings and structures in areas of abnormal stress and surveillance terrestrial laser scanners. *Life Science Journal*, *11*(9s), 165-170.

[25] Pysmenniy, S., Shvager, N., Shepel, O., Kovbyk, K., & Dolgikh, O. (2020). Development of resource-saving technology when mining ore bodies by blocks under rock pressure. *E3S Web of Conferences*, *166*, 02006. https://doi.org/10.1051/e3sconf/202016602006

[26] Matayev, A.K., Kainazarova, A.S., Arystan, I.D., Abeuov, Ye., Kainazarov, A.S., Baizbayev, M.B., Demin, V.F., & Sultanov, M.G. (2021). Research into rock mass geomechanical situation in the zone of stope operations influence at the 10th Anniversary of Kazakhstan's Independence mine. *Mining of Mineral Deposits*, *15*(1), 1-10. https://doi.org/10.33271/mining15.01.042

[27] Nurpeisova, M.B., & Kurmanbaev, O.S. (2016). Laws of devolopment of geomechanical processes in the rock mass maykain mine. *News of the National Academy of Sciences of the Republic of Kazakhstan, Series of Geology and Technical Sciences*, *6*(420), 109-115.

[28] Amralinova, B. (2023) Rare-metal mineralization in salt lakes and the linkage with composition of granites: Evidence from Burabay Rock Mass (Eastern Kazakhstan). *Water*, *15*(7), 1386. https://doi.org/10.3390/w15071386

[29] Box, S.E., Syusyura, B., Seltmann, R., Creaser, R.A., Dolgopolova, A., & Zientek, M.L. (2012). Dzhezkazgan and associated sandstone copper deposits of the Chu-Sarysu Basin, Central Kazakhstan. *Geology and Genesis of Major Copper Deposits and Districts of the World*, 1-14. https://doi.org/10.5382/sp.16.13

[30] Sultanov, M.G., Mataev, A.K., Kaumetova, D.S., Abdrashev, R.M., Kuantay, A.S., & Orynbayev, B.M. (2020). Development of the choice of types of support parameters and technologies for their construction at the Voskhod field. *Ugol*, *10*, 17-21. https://doi.org/10.18796/0041-5790-2020-10-17-21

[31] Mussin, A., Imashev, A., Matayev, A., Abeuov, Ye., Shaike, N., & Kuttybayev, A. (2023). Reduction of ore dilution when mining low-thickness ore bodies by means of artificial maintenance of the mined-out area. *Mining of Mineral Deposits*, *17*(1), 35-42. https://doi.org/10.33271/mining17.01.035

[32] Malanchuk, Z., Zaiets, V., Tyhonchuk, L., Moshchych, S., Gayabazar, G., & Dang, P. T. (2021). Research of the properties of quarry tuff-stone for complex processing. *E3S Web of Conferences*, *280*, 01003. https://doi.org/10.1051/e3sconf/202128001003

[33] Diomin, V.F., Khalikova, E.R., Diomina, T.V., & Zhurov, V.V. (2019). Studying coal seam bedding tectonic breach impact on supporting parameters of mine workings with roof bolting. *Naukovyi Visnyk Natsionalnoho Hirnychoho Universytetu*, *5*, 16-21. https://doi.org/10.29202/nvngu/2019-5/5

[34] Matayev, A.K., Musin, A., Abdrashev, R.M., Kuantay, A.S., & Kuandykova, A.N. (2021). Substantiating the optimal type of mine working fastening based on mathematical modeling of the stress condition of underground structures. *Naukovyi Visnyk Natsionalnoho Hirnychoho Universytetu*, *3*, 57-63. https://doi.org/10.33271/nvngu/2021-3/057

[35] Arystan, I.D., Baizbaev, M.B., Mataev, A.K., Abdieva, L.M., & Bogzhanova, Z.K. (2020). Selection and justification of technology for fixing preparatory workings in unstable massifs on the example of the mine "10 years of Independence of Kazakhstan. *Ugol*, *6*, 10-14. https://doi.org/10.18796/0041-5790-2020-6-10-14

[36] Haimson, B.C. (1993). The hydraulic fracturing method of stress measurement: theory and practice. *Rock Testing and Site Characterization*, 395-412. https://doi.org/10.1016/B978-0-08-042066-0.50021-5

[37] Mohamadi, A., Behnia, M., & Alneasan, M. (2021). Comparison of the classical and fracture mechanics approaches to determine in situ stress/hydrofracturing method. *Bulletin of Engineering Geology and the Environment*, *80*, 3833-3851. https://doi.org/10.1007/s10064-021-02184-8

[38] Sazid, M., Hussein, K., & Abudurman, K. (2023). Rock stress measurement methods in rock mechanics – A brief overview. *World Journal of Engineering and Technology*, *11*(2), 252-272. https://doi.org/10.4236/wjet.2023.112018

[39] Li, P., Cai, M., Miao, S., Li, Y., Sun, L., Wang, J., & Gorjian, M. (2024). Comparison and evaluation of overcoring and hydraulic fracturing stress measurements. *Scientific Reports*, *14*(1), 8771. https://doi.org/10.1038/s41598-024-59550-1

[40] Xu, C., Cui, Y., Xue, L., Chen, H., Dong, J., & Zhao, H. (2023). Experimental study on mechanical properties and failure behaviours of new materials for modeling rock bridges. *Journal of Materials Research and Technology*, *23*, 1696-1711. https://doi.org/10.1016/j.jmrt.2023.01.128

[41] Wang, C., Liu, Z., Zhou, H., Wang, K., & Shen, W. (2023). A novel true triaxial test device with a high-temperature module for thermal-mechanical property characterization of hard rocks. *European Journal of Environmental and Civil Engineering*, *27*(4), 1697-1714. https://doi.org/10.1080/19648189.2022.2092214

[42] Qi, S., Guo, S., Waqar, M. F., Luo, G., & Zhang, S. (2024). Prediction of brittle rock failure severity: An approach based on rock mass failure progress. *Journal of Rock Mechanics and Geotechnical Engineering*. https://doi.org/10.1016/j.jrmge.2024.03.005

[43] Turumbetov, T. (2022). Integrated monitoring for the rock mass state during large-scale subsoil development. *Frontiers in Environmental Science*, *10*, 852591. https://doi.org/10.3389/fenvs.2022.852591

Вивчення механічних властивостей руди та порід рудних родовищ з оцінкою природного поля напруженого стану масиву

А. Матаєв, Ш. Зейтінова, Р. Мусін, Д. Доні, Н. Шайке, А. Куттибаєв, Р. Іскаков

Мета. Проведення комплексного дослідження механічних властивостей руд та порід родовища Жиландинської групи, а також оцінка природного поля напруженого стану масиву для вирішення геомеханічних задач при оптимізації ведення гірничих робіт.

Методика. Для визначення граничних умов при вимірюванні напружено-деформованого стану масиву було запропоновано комплексну методику, що включає проведення вимірювань напружень методами гідророзриву свердловин та визначення фізико-механічних властивостей порід. Дослідженню підлягали п'ять проб гірських порід. Для кожної проби проводили дванадцять випробувань (шість випробувань у природному стані та шість – у водонасиченому).

Результати. Тести гідророзриву на вимірювальних станціях показали значні тектонічні напруження, пов'язані з формою структурних складок та тріщинуватістю масиву. Встановлено, що для масиву скельних порід характерна нерівномірна тріщинуватість. Вона має тектонічне походження та в середньому становить від 10-15 до 15-25 тріщин на метр для різних літологічних різновидів. Максимальне горизонтальне напруження на станціях орієнтовано азимутом 70° ± 10.

Наукова новизна. Для умов родовища Жиландинської групи визначено вплив водонасичення на зниження міцності та деформації гірських порід, що показало значні варіації залежно від типу породи. Особливо важливий виявлений факт суттєвого зниження міцності при одновісному стисканні та розтягуванні, а також зменшення модуля деформації й коефіцієнта зчеплення. Отримано лінійні залежності напружень за результатами вимірів, що виникають із глибиною.

Практична значимість. Отримані результати мають важливе значення для гірничодобувної галузі. Розуміння ступеня зниження характеристик міцності при водонасиченні та оцінка природного поля напруженого стану масиву дозволяє більш точно прогнозувати поведінку гірських порід.

Ключові слова: *напружений стан масиву, руда, порода, чисельний аналіз, тріщинуватість*

Publisher's note

All claims expressed in this manuscript are solely those of the authors and do not necessarily represent those of their affiliated organizations, or those of the publisher, the editors and the reviewers.